AIP | Journal of Applied Physics

Combined surface Brillouin scattering and x-ray reflectivity characterization of thin metallic films

M. G. Beghi, C. E. Bottani, P. M. Ossi, T. A. Lafford, and B. K. Tanner

Citation: J. Appl. Phys. **81**, 672 (1997); doi: 10.1063/1.364207
View online: http://dx.doi.org/10.1063/1.364207
View Table of Contents: http://jap.aip.org/resource/1/JAPIAU/v81/i2
Published by the American Institute of Physics.

Combined surface Brillouin scattering and x-ray reflectivity characterization of thin metallic films

M. G. Beghi, C. E. Bottani,[a] and P. M. Ossi
INFM–Dipartimento di Ingegneria Nucleare del Politecnico di Milano, Via Ponzio, 34/3, 20133 Milano, Italy

T. A. Lafford
Bede Scientific, Lindsey Park, Bowburn, Durham, DH6 5PF, United Kingdom

B. K. Tanner
Department of Physics, University of Durham, South Road, Durham DH1 3LE, United Kingdom

(Received 6 August 1996; accepted for publication 8 October 1996)

The structural and elastic properties of a thin gold film alloyed with Cu and Ni have been studied by surface Brillouin scattering, x-ray reflectivity and low angle x-ray diffraction. The role of guided (Sezawa) acoustic modes to determine precise values of the elastic constants has been ascertained. Although weak, the hardening effect of alloying elements has been clearly detected. © *1997 American Institute of Physics.* [S0021-8979(97)02102-6]

I. INTRODUCTION

Brillouin scattering spectroscopy of surface (SBS) acoustic phonons is currently used to investigate the elastic and structural properties of thin films and multilayers.[1–13] At the scale 1–1000 nm, this technique directly reveals the local acoustic properties of the layered medium and, from these, the elastic constants can be measured.[3–5,7,9–13,24] We stress that, in this dimensional range, SBS is the sole way[2] to obtain this last type of information. The best results have so far been obtained for semiconductor films and layered structures, in which the presence of local imperfections can be detected and characterized quantitatively.[14–19] In the case of metallic films, often poor knowledge of the precise (within, let us say, 5 nm) thickness of the film has made the estimate of elastic constants, based on SBS exclusively, unsatisfactory.[24] This imprecision has sometimes been due to unavoidable surface undulations (inhomogeneous thickness) connected with the deposition technique, and the presence of strong surface and interface roughness. Great improvements in the speed of the measurements in the presence of low SBS ripple cross sections, typical of metals, obtained by means of a new experimental apparatus, will be reported elsewhere.

In recent years, grazing angle x-ray diffraction and x-ray reflectivity have been extensively used to study the structural properties of thin films and multilayers and the topography and morphology of their surfaces and interfaces. Semiconductor-based systems have received the greatest attention because of their high *perfection* due to the special techniques by which they are produced (e.g., molecular beam epitaxy). X-ray reflectivity, in particular, can be used to evaluate film thicknesses with great precision nondestructively.

The purpose of the present work is to show that even for the less ideal metallic films the combined use of low angle x-ray and SBS techniques leads to good and useful results; the case of metallic multilayers will be presented elsewhere.[20] SBS has been used in several instances to study the surface phonon spectra of metallic surfaces and films following the development of the tandem multipass Fabry–Perot interferometer.[1] In particular, polycrystalline Au films on Si(001) were investigated in Refs. 21 and 22 and unsupported Au films in Ref. 23.

A crucial issue is that SBS is particularly successful when the geometry and the elastic symmetry of the films are known *a priori*. Here, we used x-ray reflectivity to measure the film thickness and roughness and low angle x-ray Bragg peak analysis to obtain structural information. Subsequently, the dispersion relations of several surface sagittal acoustic phonons of the film–substrate system were measured by means of SBS spectroscopy. The elastic constants of the film were obtained by fitting the theoretical dispersion relations to the experimental ones. The fit was performed using new software,[25] which also gives the layer projected densities of acoustic phonons and, in the case of very opaque films, the SBS cross section.

II. EXPERIMENTAL TECHNIQUES

A. X-ray diffraction

Film structure was determined by parallel beam thin film powder diffraction, with a Bede D3 system diffractometer with incident angle 2°, using Cu $K\alpha_1$ radiation. The x-ray tube was operated at 40 kV and 50 mA. The beam was conditioned by a 500 μm slit placed near the x-ray source, with an additional 4 mm diam pinhole before the sample. Soller slits and a graphite monochromator were positioned in front of the detector, in order to reduce, or to eliminate, peaks from the Si single crystal substrate. The detector was scanned, to give a 2θ scan, with step size 0.1° and a counting time of 3 s per point.

B. X-ray reflectivity

Measurements of thickness were made by x-ray specular reflectivity. The specular reflectivity, that is the beam reflected coherently at an angle equal to the angle of incidence,

[a]Electronic mail: Bottani@ipmce6.cesnef.polimi.it

 0021-8979/97/81(2)/672/7/$10.00

is measured by a so-called θ–2θ scan in which the detector is stepped at twice that of the specimen. Such reflectivity curves as a function of incidence angle were again measured on a D3 System diffractometer fitted with the EDRa detector.[26] The beam from the 2 kW x-ray tube was conditioned by a two-bounce, asymmetric 022 reflection, channel-cut silicon crystal.[27] The Cu $K\alpha_2$ line was removed by a slit before the sample and a 500 μm slit used before the detector to eliminate low angle diffuse scatter.

The reflectivity versus incidence angle curve is modulated with a periodicity inversely proportional to the film thickness, the constants being the wavelength of the Cu $K\alpha_1$ x-ray line and the angle. The former is known to three parts in 10^7 (Ref. 28) and the absolute precision of the D3 System angular measurement is 2 arcsec over 360°.

By fitting the x-ray reflectivity data to simulated curves, not only the film thickness but also the surface and interface roughness can be deduced. Simulations were performed using the Bede (REFS) software package,[29] which uses Parratt's recursive formalism of the Fresnel equations to calculate the reflected wave amplitude and, hence, the reflected intensity.[30] Surface and interface roughness is incorporated within the distorted Born wave approximation using a Gaussian variation of the electron density gradient.

C. Surface Brillouin scattering

Brillouin scattering spectra were recorded at room temperature in back scattering and in p-depolarized polarization conditions (incident light p-polarized, scattered light collected without polarization analysis) at several incidence angles in the range 20°–70°. With respect to the Si(001) substrate the [100] phonon propagation direction was explored. A tandem 3+3 pass high contrast interferometer of Sandercock-type[1] was used with a finesse of about 100. A free-spectral range of 16.3 GHz was adopted in the range 20°–40° and of 27.2 GHz in the range 50°–70°. The light source was an argon ion LASER Coherent Innova 300 operating in single frequency at the wavelength λ=514.5 nm. The power incident onto the sample was 100 mW. The scattered light was detected by a Hamamatsu bialkali photomultiplier tube, in a single photon counting configuration, with a dark current of 0.7 cps.

III. EXPERIMENTAL RESULTS

A film of nominal composition $Au_{90}Cu_5Ni_5$ was prepared by dc magnetron sputtering, in an Ar atmosphere, at a pressure of 0.1 Pa, with a fixed energy of 300 eV. The film, with 150 nm nominal thickness, was deposited onto a piece of Si(001) wafer, with a top native oxide layer. The sample appeared uniform, with a yellow–reddish coloration.

X-ray diffraction showed that the structure of the film is fcc, with lattice parameter a_0=0.403 76 nm±0.0009(1σ) nm; there was no evidence of film texture. Assuming equal Cu and Ni concentrations, the CuNi concentration turned out to be 8 at. %, with reference to both bulk Au and to a pure Au film, deposited by dc sputtering, adopting identical process parameters as for $Au_{92}Cu_4Ni_4$. These data imply for the mass density of the film 1.89×10^4 kg m^{-3}.

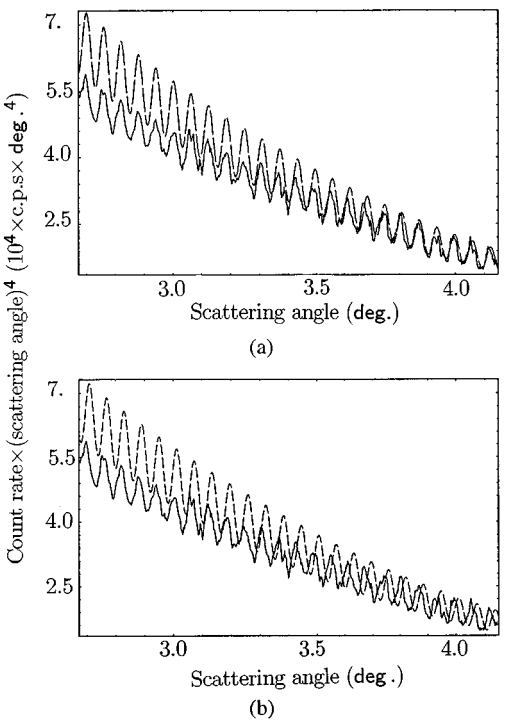

FIG. 1. (a) Experimental (solid) and simulated (dashed) reflectivity curves. The simulation assumes 134.5 nm layer thickness with 0.5 nm top surface and 0.7 nm bottom surface roughness. (b) Experimental (solid) and simulated (dashed) reflectivity curves assuming 134 nm layer thickness in the simulation.

From the Scherrer equation, grain sizes of 10 nm for $Au_{92}Cu_4Ni_4$ (111) peak and 9 nm for $Au_{92}Cu_4Ni_4$ (222) peak were obtained. The (311) peak overlapped by chance with the (331) reflection from the Si substrate peak; this resulted in an enhanced peak width that made grain size determination from this peak impossible. The (200) and (220) peaks were not observed. Due to the grain size, one order of magnitude smaller than the film thickness, elastic isotropy of the film can be assumed.

The thickness of the $Au_{92}Cu_4Ni_4$ film, measured by x-ray reflectivity, was 134.5 (±0.2) nm. Figure 1(a) shows x-ray reflectivity data and best simulated fit. A film thickness of 134.5 nm was used with top surface roughness 0.5 nm. Figure 1(b) shows a fit for film thickness 134 nm, and it is immediately clear, even without statistical treatment, that the fit is significantly worse. A thickness of 135 nm is similarly significantly worse, leading us to assign a precision of 0.2 nm to the layer thickness measurement.

Figure 2 shows the Brillouin spectrum measured at an incidence angle θ=60°. Four peaks are evident. The lowest velocity one is due to scattering from a modified Rayleigh phonon (mR), while all other peaks are associated with Sezawa phonons (S) of increasing order. All the above phonons have a parallel wave vector that is given by $q_\parallel=(4\pi/\lambda)\sin\theta$ (Ref. 16) and possess a sagittal polarization with both shear vertical (z) and longitudinal (x) components in their displacement field. As a general rule, the mR phonon penetrates deeper in the substrate (with a penetration depth of about $2\pi/q_\parallel$, i.e., 297 nm at θ=60°) and it would exist

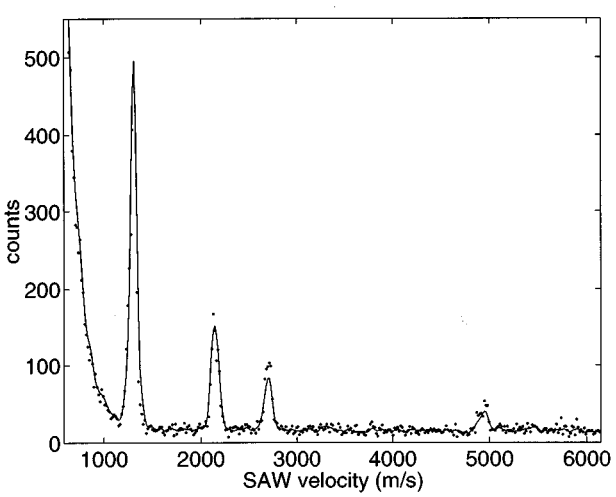

FIG. 2. Measured Brillouin spectrum at the incidence angle $\theta=60°$.

even in the absence of the film as a pure Rayleigh wave of the Si surface. The Sezawa phonons instead are essentially guided waves in the film, even though they have a tail extending in the substrate.

Not all the Sezawa phonons with the given $q_{\parallel}$ are visible in Fig. 2, as it will be shown below. Gold exhibits a significant volume elasto-optic effect but, due to its metallic opacity [its skin depth at 514.5 nm is $\approx$14 nm (Ref. 31)] the Brillouin cross section is, in our case, mainly attributable to the surface ripple effect.[21] Phonons polarized in the shear horizontal (y) direction have, therefore, a negligible cross section, while the ripple cross section of sagittal phonons is proportional to the thermal average of the power spectrum of the total vertical component of the phonon displacement field at the outer surface of the film. Figure 3(a) shows such a power spectrum computed using the best-fit values for both film thickness and acoustic properties (see below). In Fig. 3(b) the power spectrum of the longitudinal component is also shown. The spectra are obtained, using the fluctuation–dissipation theorem, from the phonon Green functions[32] $G_{zz}(z,z'|\omega-i\epsilon,q_{\parallel})$ and $G_{xx}(z,z'|\omega-i\epsilon,q_{\parallel})$, using new software reported elsewhere.[33] The dependence of these spectra on depth is shown in Fig. 4 by means of the contour plots of the layer projected phonon density of states (LPPDS), both for x and for z polarizations. For any given polarization the LPPDS represent the contribution to the normal modes with parallel velocity between v and $v+dv$ arising from the atoms that lie in the infinitesimal layer of thickness dz, located at depth z.

From inspection of Fig. 3 and 4 it is evident that there are six Sezawa phonons (plus the mR one) in this film. Yet, Fig. 3(a) shows clearly why Sezawa phonons of order 3, 4, and 6, having at the surface a mainly longitudinal polarization, are less visible than the mR phonon and Sezawa phonons of order 1, 2, and 5. The presence of a volume elasto-optic contribution to the cross section explains why the experimental intensity ratios among the various peaks do not agree perfectly with the theoretical prediction of Fig. 3(a) based only on the ripple effect.

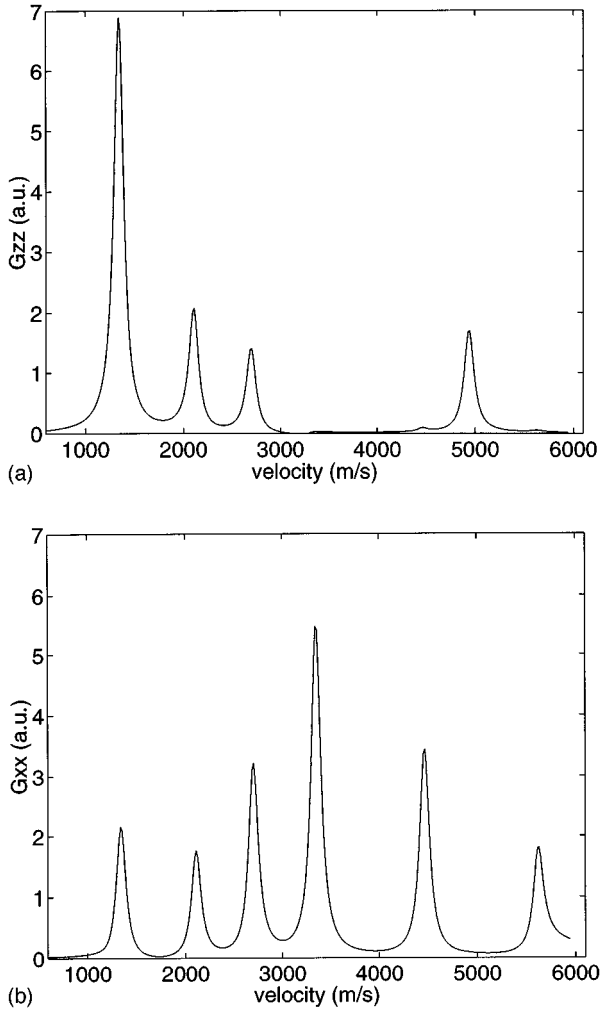

FIG. 3. Power spectra of the phonon displacement field at the outer surface of the film, for $q_{\parallel}=0.021\,15\ \mathrm{nm}^{-1}$, corresponding to the incidence angle $\theta=60°$: (a) vertical (z) component, (b) longitudinal (x) component.

IV. DERIVATION OF THE ELASTIC CONSTANTS

The phase velocities of surface acoustic waves (SAWs) were computed for a silicon substrate whose acoustic properties are:[16] $C_{11}=166$ G Pa, $C_{12}=63.9$ G Pa, $C_{44}=79.6$ G Pa, $\varrho=2.33\ 10^3$ kg m^{-3}, and for a homogeneous surface layer of thickness $h=134.5$ nm. As already noted, x-ray analysis shows that the layer can be assumed to be isotropic. For reference purposes, the properties of a pure gold layer are:[23] $C_{11}=207$ G Pa, $C_{44}=25.0$ G Pa, and $\varrho=19.75\ 10^3$ kg m^{-3}, corresponding to a Young modulus $E=71.6$ G Pa and a shear modulus $G=25.0$ G Pa.

The phase velocities of SAWs were computed by the so-called mode-matching method:[34] the displacement field $\mathbf{u}(x,y,z)=(u_x,u_y,u_z)$ of a SAW propagating along x on a surface coincident with the (x,y) plane is independent of y and proportional to $\exp[i(q_{\parallel}x+q_{\perp}z)]$, where the real $q_{\parallel}$ and complex $q_{\perp}$ are the components of the wave vector parallel and perpendicular to the surface. For high symmetry directions like the [100] considered here, the sagittal modes polarized in the (x,z) plane, decouple from the shear horizontal modes, polarized along the y direction. In each homogeneous

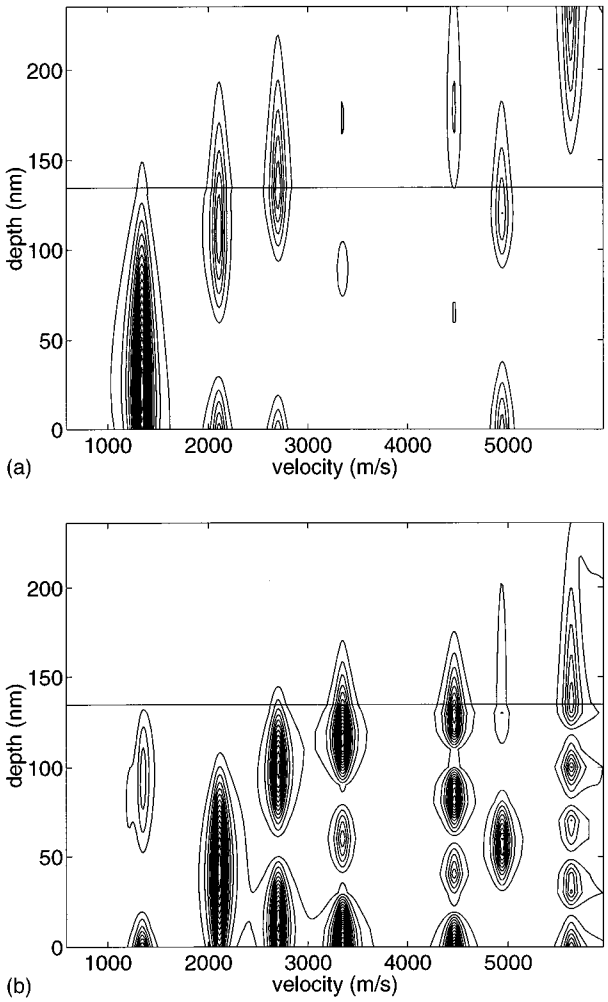

FIG. 4. Layer projected phonon density of states (LPPDS) of the phonon displacement field, as a function of velocity and depth, for $q_{\parallel}=0.021\,15$ nm^{-1}, corresponding to the incidence angle $\theta=60°$: (a) vertical (z) component, (b) longitudinal (x) component. The horizontal line marks the film/substrate interface.

layer the dispersion relation $q_{\perp}=q_{\perp}(q_{\parallel},\omega)$ is easily found, and the boundary conditions, i.e., the vanishing of the normal components of the stress tensor at the free surface and the continuity of displacements and stresses at the interface, take the form of a homogeneous system of equations. The determinant of the coefficients of this system is a function of $q_{\parallel}$ and ω, parametrically depending on the geometry (film thickness h) and acoustic properties (mass densities ϱ and elastic constants C_{ij}); its zeros, as functions of $q_{\parallel}$, identify the dispersion relations of the true surface modes (nonleaky modes).

Adopting the previously indicated values for the properties of the silicon substrate and for the film thickness, the dispersion relations $c_m=c_m(q_{\parallel},\varrho,C_{ij})$ depend only on the mass density and elastic constants of the film (c_m are the phase velocities of the acoustic modes). The elastic constants can be represented by the Young's modulus E and the shear modulus G: $c_m=c_m(q_{\parallel},\varrho,E,G)$. One branch of the dispersion relation can be fitted to the velocities $c_m^m(q_{\parallel n})$ measured at the given set $\{q_{\parallel n}\}$, by minimizing the least-squares residual function

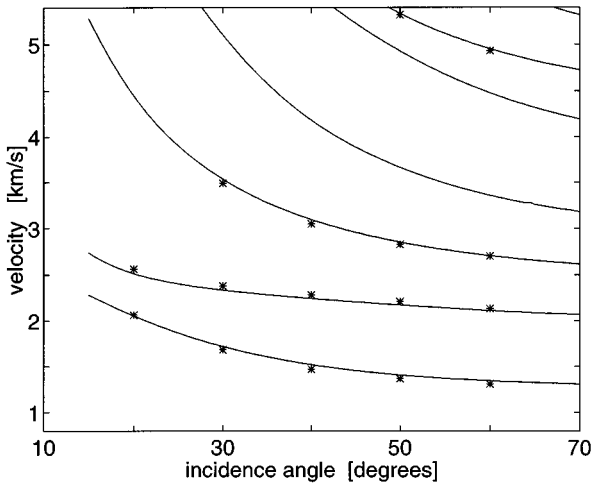

FIG. 5. Experimental (isolated points) and computed (continuous lines) dispersion relations of the various surface phonons, for the mass density of the film measured by x rays and the elastic constants obtained by best-fit procedure.

$$R_m^2(\varrho,E,G)=\sum_{n=1}^{N}\,[c_m^m(q_{\parallel n})-c_m(q_{\parallel n},\varrho,E,G)]^2, \quad (4.1)$$

and the acoustic properties of the film are estimated by minimizing the total residual function

$$R(\varrho,E,G)=\sqrt{\sum_{m=1}^{M} R_m^2}. \quad (4.2)$$

The minimum of R is found at the values $\varrho=1.91\times10^4$ kg m^{-3}, $E=81.6$ G Pa, and $G=28.8$ G Pa. The value of the density compares well with the value $\varrho_X=1.89(\pm0.01)\times10^4$ kg m^{-3} obtained from the x-ray measurements. Furthermore, in the neighborhood of the minimum, the residual R function has little sensitivity to the value of ϱ: if minimization is performed only with respect to E and G, keeping fixed $\varrho=\varrho_X$ (about 1% smaller than the above value), the minimum is found at $E=80.6$ G Pa and $G=28.4$ G Pa (slightly more than 1% smaller than the above values), with the residual function R increased by only 0.17%. The measurement of the density by x rays is, thus, more precise than the derivation by the fitting procedure, therefore, in the following we keep fixed $\varrho=\varrho_X=18.916\times10^3$ kg m^{-3}; accordingly, the minimum of R is obtained for $E=80.58$ G Pa and $G=28.41$ G Pa. Figure 5 shows good agreement between the experimental dispersion relations and the theoretical curves computed with the above values of the mass density and elastic constants of the film.

In order to assess the accuracy and significance of the above values of E and G, the residual functions R_ms and R have been computed as a function of E and G,[24] with $\varrho=\varrho_x$. Figures 6(a) and 6(b) show the contour maps of R_1, corresponding to the modified Rayleigh wave, and R_2, corresponding to the first Sezawa wave, while Figs. 6(c) and 6(d) show the map for the total residual function R. The considered intervals for E and G are 76–83 G Pa and 25.5–29.5 G Pa, respectively. Part of this domain violates the thermo-

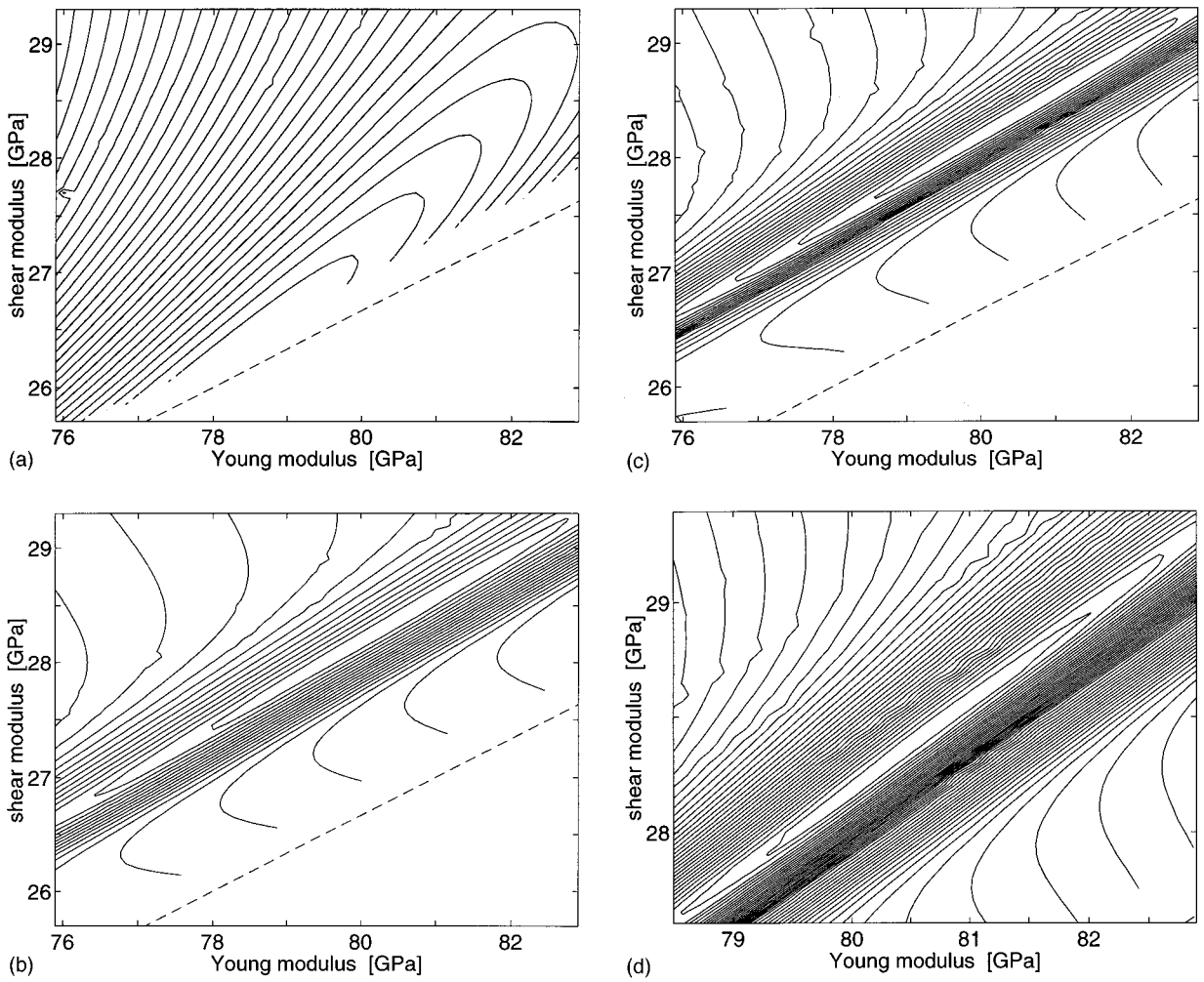

FIG. 6. (a) Normalized residual function field $R_1(E,G)/R_{1(\min)}$ corresponding to the modified Rayleigh wave. Contour lines are drawn for $R_1/R_{1(\min)}=1$, 1.1, 1.2,.... (b) Normalized residual function field $R_2(E,G)/R_{2(\min)}$ corresponding to the first Sezawa wave. Contour lines are drawn for $R_2/R_{2(\min)}=1$, 1.5, 2,.... (c) Normalized total residual function field $R(E,G)/R_{(\min)}$. Contour lines are drawn for $R/R_{(\min)}=1$, 1.2, 1.4,.... (d) Magnification of (c) with contour lines drawn for $R/R_{(\min)}=1$, 1.1, 1.2,....

dynamic stability condition $\nu \leqslant 1/2$, i.e., $G \geqslant E/3$;[35] the frontier of the unphysical domain is indicated by the dashed line, and computations were not pushed up to the frontier because, approaching it, the C_{11} elastic constant diverges. Furthermore, when the elastic constants approach more closely the frontier, the film no longer supports all the observed Sezawa modes.

The contour lines are plotted for values normalized to the minimum value of each residual function $R_m/R_{m(\min)}$. Note that the different residual functions R_ms show different sensitivities to E and G values, and in order to obtain readable maps contour lines have to be plotted for different intervals of the ratio $R_m/R_{m(\min)}$.

R_1, corresponding to the modified Rayleigh wave, does not exhibit a sharp minimum, but only a wide depression, which declines towards the unphysical region [see Fig. 6(a)]. This behavior can probably be attributed to the fact that, among all the surface waves, the Rayleigh one is the most penetrating into the substrate. As we have a soft film on a hard substrate, the stiffness of the mode is mainly provided by the substrate, while the film plays a role that approaches that of a mass loading.

R_2, corresponding to the first Sezawa wave, has instead the shape of a sharp valley; the bottom of the valley follows a straight line along which the values of R_2 have only small and smooth variations [see Fig. 6(b)]. The behavior of R_3, corresponding to the second Sezawa wave, is very similar to that of R_2: the bottom of the two valleys coincides, although the weak minima of R_2 and R_3 fall at different locations. R_4 instead, corresponding to the fifth Sezawa wave has a wide and shallow minimum, mainly due to the presence of only two experimental points on that branch.

The behavior of the total residual function R is dominated by that of R_2 and R_3: it has the shape of a sharp valley, whose bottom follows the line $G=28.41+0.3843\times(E-80.58)$ (E, G in G Pa). It can be seen from the Fig. 6(c) and 6(d) that this linear relation between E and G is established to a high degree of accuracy. Along this line the minimum, at $E=80.58$ G Pa and $G=28.41$ G Pa, is localized with a lower precision, and it is more safely located in the interval be-

TABLE I. Values of E and G that minimize $R(\varrho_X,E,G)$, and values of ϱ, E, and G that minimize $R(\varrho,E,G)$, for the given values of film thickness h. For $h=130$ nm two minima of $R(\varrho,E,G)$ are found, having very similar depths.

h (nm)	fixed ϱ (kg m^{-3})	fitted ϱ (kg m^{-3})	E (G Pa)	G (G Pa)
130	18 916		78.03	27.55
130		19 683	81.75	28.87
130		19 828	82.49	29.13
134.5	18 916		80.58	28.41
134.5		19 122	81.61	28.77
139	18 916		83.03	29.26
139		18 549	81.19	28.56

tween $E=79.5$ G Pa and $E=81.5$ G Pa; according to the linear relation between E and G, G lies in the interval 28–28.76 G Pa, and the Poisson ratio $\nu=(E/2G)-1$ lies in the interval 0.4200–0.4168. Such values for E and G are higher than those of a pure gold film;[23] alloying with copper and nickel has the effect of increasing the stiffness of gold.

It is, thus, shown that by exploiting the information from all branches (including the fifth Sezawa mode) the linear relation between E and G is confirmed and the uncertainties on their values are reduced below 2%, corresponding for ν to an uncertainty below 1%. It has recently been shown[24] that the knowledge of the dispersion relations of Rayleigh and Love waves is particularly effective to this purpose, but in this opaque film the Love modes cannot be observed.[16] Yet, the measurement of both Rayleigh and Sezawa modes allows us, although with a lower efficiency, to reduce significantly the uncertainties in the derivation of the elastic constants. The values for the elastic constants depend critically on the thickness of the film, the value of which must be determined independently, for example by x-ray reflectivity.

To assess quantitatively the importance of accurate measurements of film thickness, the fitting procedure has been repeated adopting thickness values of 130 and 139 nm, instead of the measured 134.5 nm, and either leaving the mass density of the film as a fit parameter, or fixing it at the value $\varrho=\varrho_x$. The results are presented in Table I. It must be noted that for $h=130$ nm two minima of $R(\varrho,E,G)$ are found, having almost exactly the same depth, and that for all values of h the minimum of $R(\varrho,E,G)$ is smaller than the minimum of $R(\varrho_x,E,G)$ by less than 2%, confirming the weak sensitivity of R on ϱ, at least in the neighborhood of the minimum.

Looking at Table I it can be seen that ϱ must be given the ϱ_x value, leading to a relative error for the elastic constants of the same order of that of thickness measurement. The importance of x-ray measurement of both density and thickness is evident.

V. CONCLUSIONS

The nondestructive nature of both x-ray scattering and SBS must be put forward. In fact, the required structural characterization of the film could also be obtained by cross-sectional transmission electron microscopy (TEM) analysis but in a completely destructive and time consuming way. Furthermore, sometimes metallic systems on semiconductor substrates (e.g., Au on Si) exhibit poor adhesion and the procedure needed to prepare the TEM sample could easily cause the film to delaminate.

We have shown that the combined use of SBS and x-ray reflectivity is effective to determine the elastic properties of thin metallic films. The method has proved to be sensitive enough to detect the small hardness increase as induced in a gold film by a small content of alloying elements.

ACKNOWLEDGMENTS

Thanks are expressed to A. Mantegazza for the SBS measurements. Professor L. A. Guzman is gratefully acknowledged for providing the films. One of the authors (P. M. O.) acknowledges support by the Italian Ministero dell'Università e della Ricerca Scientifica (MURST).

[1] F. Nizzoli and J. R. Sandercock, in *Dynamical Properties of Solids*, edited by G. K. Horton and A. A. Maradudin (Elsevier Science, Amsterdam, 1990), Vol. 6, p. 281.
[2] P. Mutti, C. E. Bottani, G. Ghislotti, M. Beghi, G. A. D. Briggs, and J. R. Sandercock, in *Advances in Acoustic Microscopy*, edited by G. A. D. Briggs (Plenum, New York, 1995), p. 249.
[3] L. Sun, J. R. Dutcher, L. Giovannini, F. Nizzoli, J. R. Stevens, and J. L. Ord, J. Appl. Phys. **75**, 7482 (1994).
[4] H. von Känel, M. Mendik, K. A. Mäder, N. Onda, S. Goncalves-Conto, C. Schwarz, G. Malegori, L. Miglio, and F. Marabelli, Phys. Rev. B **50**, 3570 (1994).
[5] S. Subramanian, R. Sooryakumar, G. A. Prinz, B. T. Jonker, and Y. U. Idzerda, Phys. Rev. B **49**, 17 319 (1994).
[6] Hua Xia, G. Carlotti, G. Socino, K. J. Chen, Wei Zhang, Z. F. Li, and X. K. Zhang, J. Appl. Phys. **75**, 475 (1994).
[7] Hua Xia, Wei Zhang, X. X. Qu, Jun Zhang, J. G. Jiang, and Rong Zhang, Phys. Status Solidi A **140**, 429 (1993).
[8] X. Jiang, J. W. Zou, K. Reichelt, and P. Grünberg, J. Appl. Phys. **66**, 4729 (1989).
[9] X. Jiang, B. Goranchev, K. Schmidt, P. Grünberg, and K. Reichelt, J. Appl. Phys. **67**, 6772 (1990).
[10] X. Jiang, J. Fassbender, and B. Hillebrands, Phys. Rev. B **49**, 13 815 (1994).
[11] S. Lee, B. Hillebrands, G. I. Stegeman, H. Cheng, J. E. Potts, and F. Nizzoli, J. Appl. Phys. **63**, 1914 (1988).
[12] M. Grimsditch, E. S. Zouboulis, and A. Polian, J. Appl. Phys. **76**, 832 (1994).
[13] A. Neubrand and P. Hess, J. Appl. Phys. **71**, 227 (1992).
[14] C. E. Bottani, G. Ghislotti, and P. Mutti, J. Phys., Condens. Matter. **6**, L85 (1994).
[15] V. V. Aleksandrov, C. E. Bottani, G. Caglioti, G. Ghislotti, C. Marinoni, P. Mutti, N. L. Yakovlev, and N. S. Sokolov, J. Phys., Condens. Matter. **6**, 1947 (1994).
[16] F. Nizzoli, C. Byloos, L. Giovannini, C. E. Bottani, G. Ghislotti, and P. Mutti, Phys. Rev. B **50**, 2027 (1994).
[17] G. Ghislotti and C. E. Bottani, Phys. Rev. B **50**, 12 131 (1994).
[18] G. Ghislotti, C. E. Bottani, P. Mutti, C. Byloos, L. Giovannini, and F. Nizzoli, Phys. Rev. B **51**, 9875 (1995).
[19] G. Ghislotti, A. Gagliardi, C. E. Bottani, S. Bertoni, G. F. Cerofolini, and L. Meda, Mater. Sci. Eng. B **36**, 129 (1996).
[20] M. Beghi, C. E. Bottani, P. M. Ossi, and B. X. Liu (unpublished).
[21] L. Bassoli, F. Nizzoli, and J. R. Sandercock, Phys. Rev. B **34**, 1296 (1986).
[22] B. Hillebrands, R. Mock, G. Güntherodt, P. S. Bechthold, and N. Herres, Solid State Commun. **60**, 649 (1986).
[23] M. Grimsditch, R. Bhadra, and I. K. Schuller, Phys. Rev. Lett. **58**, 1216 (1986).
[24] S. Makarov, E. Chilla, and H. J. Frölich, J. Appl. Phys. **78**, 5028 (1995).
[25] M. Beghi and C. E. Bottani (unpublished).
[26] S. Cockerton and B. K. Tanner, Adv. X-ray Anal. **38**, 371 (1995).
[27] N. Loxley, B. K. Tanner, and D. K. Bowen, J. Appl. Crystallogr. **28**, 314 (1995).
[28] J. Härtwig, S. Grosswig, P. Becker, and D. Windisch, Phys. Status Solidi A **125**, 79 (1991).

[29] M. Wormington, D. K. Bowen, and B. K. Tanner, Mater. Res. Soc. Symp. Proc. **238**, 119 (1991).
[30] L. G. Parratt, Phys. Rev. **95**, 359 (1954).
[31] R. Loudon, Phys. Rev. Lett. **40**, 581 (1978).
[32] M. G. Cottam and A. A. Maradudin, in Surface Excitations, edited by V. M. Agranovich and R. Loudon (North Holland, Amsterdam, 1984), p. 1.
[33] M. Beghi, C. E. Bottani, and A. Romaniello (unpublished).
[34] G. W. Farnell and E. L. Adler, in *Physical Acoustics*, edited by W. P. Mason and R. N. Thurston (Academic, New York, 1972), Vol. 9.
[35] L. D. Landau and E. M. Lifshitz, *Theory of Elasticity* (Pergamon, 1970).